Dynamic Modeling and Simulation of a Multiport DC Hub with Closed Loop Control

Luo Liu, Xianghua Shi, Shaahin Filizadeh, David Jacobson

***Abstract*—The paper presents a dynamic average-value model for a multi-port dc interconnection hub based upon the concept of generalized averaging method (i.e., dynamic phasors). The model is able to predict the transient and steady state response of a dc hub and its closed loop control system with accuracy and markedly higher computational efficiency than a conventional EMT model. Simulations results are presented for a three-port dc hub and are compared with detailed EMT results from PSCAD/EMTDC.**

***Keywords*: Dynamic modeling, dc grids, dynamic phasor, simulation, dc hubs.**

I. Introduction

With the increasing demand for generation of clean energy from renewable energy resources, such as offshore wind farms and solar farms, research and development on dc power grids, especially with high- or medium-power dc-dc converters, has attracted much attention. Conventional ac power systems have been operating for several decades with little or no significant dc subsystems. DC systems, however, have been gaining increasing appeal due to the proliferation of such technologies as solar power generation and bulk energy storage, both of which are dc in nature. It is, therefore, necessary to investigate how these primarily dc systems are to be interconnected to existing ac power systems. Meanwhile, there is a need to develop means for interconnection of large dc subsystems together as they become more prevalent and the concept of dc grids becomes a closer reality.

An important issue to address is how to integrate multiple dc grids (or subsystems) with different voltage levels. Several multiport dc-dc converters for use in high-medium power systems have been proposed and studied in the past [1]-[7]. In [7], a multiport high power LCL dc hub, as shown in Fig. 1, is proposed based upon the idea of an LCL resonant converter [8]. The dc hub has a multiport configuration and can be used as the interconnection point of different dc voltages. Each port has the ability of bidirectional power flow and operates independently from the other ports. Power flow may occur among different networks. The power exchange point is an ac bus, which only connects different LCL resonant tanks with a relatively high fundamental frequency so that the size of inductive components can be reduced. Another key advantage of this topology is the ability to add new ports to the dc hub without making any component changes to the other ports.

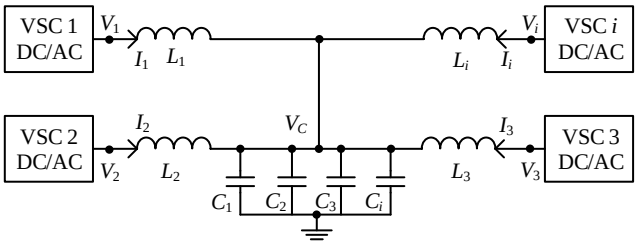

Fig. 1. DC hub structure [7].

In [9], a two-port dc hub has been prototyped with closed loop control to validate the topology from [7]. However, several questions regarding the control of a multiport dc hub remain unanswered. Moreover, [10] states that simulating such a dc hub with a medium fundamental frequency (200-2000 Hz) in an electromagnetic transient (EMT) simulation software, such as PSCAD/EMTDC, requires extremely small time-steps to achieve sufficient accuracy due to the numerical instability that may result from the one time-step delay when the EMT solver performs numerical integration of the control systems and the vector angle delay associated with the *dq0* transformations. The proposed solutions in [10] for these two problems are to avoid the time-step delay in the numerical integration and to compensate the vector angle delay of the *dq0* transformations. By applying the proposed solutions, [10] reports significant improvements in the speed and accuracy of simulating a medium-frequency two-port dc hub. However, these methods have not yet been tested on a multiport dc hub with closed loop control.

This paper firstly proposes an average-value model in the *dq* domain for a multiport dc hub; the model significantly accelerates the simulation speed of a dc hub by several orders of magnitude. Secondly, and for the first time to the best of the authors' knowledge, control methods of the two-port dc hub in [9] are extended to a multiport hub. The averaged model and the closed loop control algorithms are validated against detailed EMT simulation results in PSCAD/EMTDC.

II. Operating Principles and Control System

A. Operating Principles

The voltage source converters (VSCs) in the dc hub can be of any type including two-level, multi-level, or modular multilevel converters. According to design principles in [7], the values of LCL filter components are selected based on

This work was sponsored in part by the University of Manitoba, by Manitoba Hydro, and by MITACS Accelerate Program.

Luo Liu, Xianghua Shi and Shaahin Filizadeh are with Department of Electrical and Computer Engineering, University of Manitoba, Winnipeg, MB, Canada (e-mail of corresponding author: shaahin.filizadeh@umanitoba.ca).
David Jacobson is with Manitoba Hydro, Winnipeg, MB, Canada (e-mail: dajacobson@hydro.mb.ca).

Paper submitted to the International Conference on Power Systems Transients (IPST2019) in Perpignan, France June 17-20, 2019.

factors such as the rated power, dc link voltages, number of ports, operating frequency, considerations of resonant frequency, and so on. Since the application of a dc hub is mainly for connecting multiple dc links, the internal harmonics of a dc hub are not a significant concern. Basic operating principles of a dc hub under normal conditions are illustrated in [7] and summarized as follow.

a. The voltage and current of each port are in phase; therefore, all ports operate at unity power factor to reduce the currents drawn and losses;
b. The phase of voltage across the parallel capacitors, V_C, is considered as reference angle, so that $V_{Cq} = 0$;
c. As a result, the zero summation of *d* components of the port currents indicates power balance in a dc hub.

In any circuit, the complex power is presented as follows.

$$S = VI^* = P + jQ \tag{1}$$

In *dq* domain, any vector (denoted as *X*), is represented as:

$$X = X_d + jX_q \tag{2}$$

The complex power can, therefore, be re-written as follows.

$$\begin{aligned} S &= (V_d + jV_q)(I_d - jI_q) \\ S &= V_d I_d + V_q I_q + j(V_q I_d - V_d I_q) \end{aligned} \tag{3}$$

Thus, the port current shown in Fig. 1 is given in (4).

$$I_i = \frac{V_i - V_C}{j\omega L_i} = \frac{V_{id} + jV_{iq} - V_{Cd} - jV_{Cq}}{j\omega L_i} \tag{4}$$

where V_i is the port voltage. As mentioned earlier, V_{Cq} is forced to be zero, which implies that (4) can be simplified as:

$$I_i = I_{id} + jI_{iq} = \frac{V_{iq}}{\omega L_i} + j\frac{V_{Cd} - V_{id}}{\omega L_i} \tag{5}$$

According to (3) and with V_{Cd} equal to V_C, the port's real power is

$$P_i = V_{id} I_{id} + V_{iq} I_{iq} = \frac{V_{iq} V_{Cd}}{\omega L_i} = I_{id} V_C \tag{6}$$

Based on (6), the I_{id} component of the port current controls the real power as V_C is left to be an uncontrolled variable, although the magnitude of V_C may be impacted by the variation of port current. In (5), it is clear that I_{id} can be controlled by V_{iq} or effectively the *q* component of the modulation index since port voltages can be expressed as follows.

$$V_i = V_{id} + jV_{iq} = M_{id} E_i + jM_{iq} E_i \tag{7}$$

where M_{id} and M_{iq} are the modulation indices for *dq* components of the port voltages, respectively.

B. Controller Design

According to the operating principles summarized above, a three-port dc hub control system is shown in Fig. 2. The concept of this control is based on the two-port dc hub control method proposed in [9]. Similar to the two-port dc hub control, there are six inner loops to control the *dq* components of port currents. Each I_{iq} reference is computed based on its corresponding I_{id} reference and the phase angle to ensure that the port operates at unity power factor. However, the power references to the outer loops are given individually except for one power that must balance the total power.

For instance, in Fig. 2, P_{2ref} and P_{3ref} are given individually to generate the I_{id} references for these two ports. However, I_{1ref} is computed directly based on the I_{id} reference for other ports since the sum of I_{id} must be zero to force V_{cq} to be zero (which is the true condition for achievement of power balance). The reason for not adding another set of PI controller to generate I_{1d} references based on P_{1ref} is that in reality the dc hub will not be lossless; the sum of port powers is not zero if losses are considered, as ports powers must be slightly adjusted to account for the internal losses of the hub. This control design can be extended to a larger number of ports. In such a case, all inner loop controllers will remain unchanged. All I_{id} references are the output of the power control loops except only one for which the I_{id} reference is automatically known from other I_{id} references. Although the harmonics in the dc hub do not play any roles in power conversion or power quality, they will bring challenges to the controllers. The harmonics will generate considerably large ripples and oscillations on the *dq* components after performing *dq0* transformation. As a consequence, filters are added in the control loops to filter out ripples on the *dq* components of the port currents.

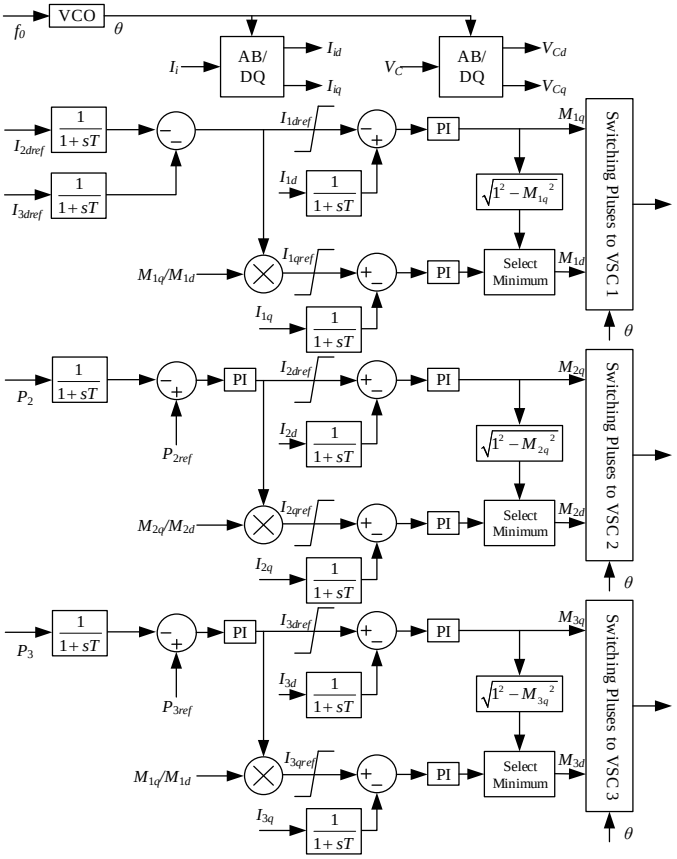

Fig. 2. Control system of three-port dc hub.

III. Modeling of a Three-Port DC Hub

Since the control system only processes and controls the *dq* components, it is not beneficial to simulate the dc hub in the original *abc* domain. For example, the default simulation mode in PSCAD/EMTDC uses nodal analysis for the power circuit components and the currents and voltages are in the

original *abc* domain. To process the control system, all signals in the *abc* domain must be converted into a *dq* frame. However, performing *dq* transformation will cause a small angle delay for signals in the *dq* components [10]. This angle delay may not be significant for a low-frequency system (e.g., 60 Hz); however, it will have a considerable impact on the phase angle information if the base frequency is large (e.g., 1 kHz).

Harmonic contents of the dc hub may be reduced using higher switching frequencies, MMC topologies, or optimal pulse width modulation (OPWM) methods. The focus of this paper will be on the fundamental component dynamics of the dc hub, and the average-value model in this paper is developed for this purpose. A three-port dc hub is investigated and the VSCs are considered as ac sources in the averaged model depicted in Fig. 3; C_{eq} is the sum of all parallel capacitors.

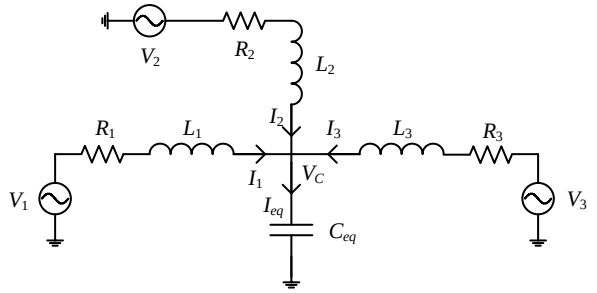

Fig. 3. Three-port dc hub in the averaged model.

A. Circuit Modeling

To model this circuit, the concept of generalized averaging method [11] is employed. Each *abc*-domain variable is approximated with its fundamental component, which itself is represented by its time-varying Fourier coefficients (or *dq* components) as follows.

$$x(t) = x_d + jx_q \tag{8}$$

The *dq* components are, in general, functions of time because of the transients in the original variables. The following expression is useful in modeling using the generalized averaging concept.

$$\frac{d}{dt}\langle x\rangle_k(t) = \langle \frac{d}{dt}x\rangle_k(t) - jk2\pi f\langle x\rangle_k \tag{9}$$

where f is the frequency of the fundamental component.

The dc hub may be controlled using the magnitude and phase of each converter output, or in other words the *dq* components of the port voltages. Thus, the state space equations for the ac part of the hub are as follows.

$$\frac{d}{dt}I_{id} = \frac{1}{L_i}(V_{di} + \omega L_i I_{iq} - V_{Cd} - R_i I_{id}) \tag{10}$$

$$\frac{d}{dt}I_{iq} = \frac{1}{L_i}(V_{qi} - \omega L_i I_{id} - V_{Cq} - R_i I_{iq}) \tag{11}$$

$$\frac{d}{dt}V_{Cd} = \frac{1}{C_{eq}}(I_{Cd} + \omega C_{eq} V_{Cq}) \tag{12}$$

$$\frac{d}{dt}V_{Cq} = \frac{1}{C_{eq}}(I_{Cq} - \omega C_{eq} V_{Cd}) \tag{13}$$

where $i = 1,2,3$, and I_{id} and I_{iq} are the *dq* components of port currents; I_{Cd} and I_{Cq} are the *dq* components of the current through the equivalent capacitor C_{eq}, and they are the sum of I_{id} and I_{iq} on all ports, respectively; R_i and L_i are the resistance and inductance at each port, respectively. Therefore, the state space equations can be written in the matrix form as follows.

$$\frac{d}{dt}\begin{bmatrix} I_{1d} \\ I_{1q} \\ I_{2d} \\ I_{2q} \\ I_{3d} \\ I_{3q} \\ V_{Cd} \\ V_{Cd} \end{bmatrix} = \boldsymbol{A}\begin{bmatrix} I_{1d} \\ I_{1q} \\ I_{2d} \\ I_{2q} \\ I_{3d} \\ I_{3q} \\ V_{Cd} \\ V_{Cd} \end{bmatrix} + \boldsymbol{B}\begin{bmatrix} V_{1d} \\ V_{1q} \\ V_{2d} \\ V_{2q} \\ V_{3d} \\ V_{3q} \end{bmatrix} \tag{14}$$

where $\boldsymbol{A}$ and $\boldsymbol{B}$ are expressed as

$$\boldsymbol{A} = \begin{bmatrix} -\frac{R_1}{L_1} & \omega & 0 & 0 & 0 & 0 & -\frac{1}{L_1} & 0 \\ -\omega & -\frac{R_1}{L_1} & 0 & 0 & 0 & 0 & 0 & -\frac{1}{L_1} \\ 0 & 0 & -\frac{R_2}{L_2} & \omega & 0 & 0 & -\frac{1}{L_2} & 0 \\ 0 & 0 & -\omega & -\frac{R_2}{L_2} & 0 & 0 & 0 & -\frac{1}{L_2} \\ 0 & 0 & 0 & 0 & -\frac{R_3}{L_3} & \omega & -\frac{1}{L_3} & 0 \\ 0 & 0 & 0 & 0 & -\omega & -\frac{R_3}{L_3} & 0 & -\frac{1}{L_3} \\ \frac{1}{C_{eq}} & 0 & \frac{1}{C_{eq}} & 0 & \frac{1}{C_{eq}} & 0 & 0 & \omega \\ 0 & \frac{1}{C_{eq}} & 0 & \frac{1}{C_{eq}} & 0 & \frac{1}{C_{eq}} & -\omega & 0 \end{bmatrix}$$

$$\boldsymbol{B} = \begin{bmatrix} \frac{1}{L_1} & 0 & 0 & 0 & 0 & 0 \\ 0 & \frac{1}{L_1} & 0 & 0 & 0 & 0 \\ 0 & 0 & \frac{1}{L_2} & 0 & 0 & 0 \\ 0 & 0 & 0 & \frac{1}{L_2} & 0 & 0 \\ 0 & 0 & 0 & 0 & \frac{1}{L_3} & 0 \\ 0 & 0 & 0 & 0 & 0 & \frac{1}{L_3} \\ 0 & 0 & 0 & 0 & 0 & 0 \\ 0 & 0 & 0 & 0 & 0 & 0 \end{bmatrix}$$

In the state space equations, all the state variables are dc quantities in steady state; during transients the variations of *dq*

components represent the changes in the magnitude and phase angle of the fundamental component of the respective variable. The above differential equations can be solved numerically using a suitable integration method. Since the system of equations in (14) is linear, the trapezoidal integration method may be applied readily.

B. Control Processing

In a linear system, controllers may be written directly into the state space equations and become a part of ***A*** and ***B*** matrices. However, the control system of a dc hub is nonlinear; linearization around an operating point may be used at the expense of losing large-signal representability. In this work, the nonlinear control system is formulated and solved separately from the linear systems equations. This allows the use of different integration methods, e.g., trapezoidal method for linear system equations and Euler's method for the nonlinear controls.

A proportional-integral (PI) controller is shown in Fig. 4.

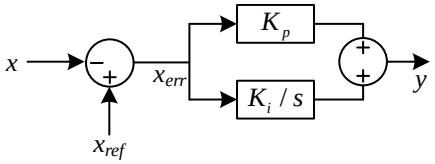

Fig. 4. Block diagram of a PI controller.

The input of the PI controller is

$$x_{err}(t) = x_{ref} - x(t) \tag{15}$$

where x is the controlled variable and x_{ref} is the desired reference. The output of the PI controller is

$$y(t) = K_p x_{err}(t) + \int K_i x_{err}(t)dt \tag{16}$$

where K_p and K_i are the gains of the PI controller. With

$$a(t) = \int K_i x_{err}(t)dt \tag{17}$$

Euler's method may be used to implement the integration with proper saturation limits in place for those in both $a(t)$ and the PI controller output $y(t)$. Moreover, the transfer functions of all filters in the control system are in the same form as shown below,

$$G_f(s) = \frac{1}{1+sT} \tag{18}$$

where T is the time constant of the filter. This first-order differential equation may also be solved using either of the two integration methods.

IV. Simulation Results and Comparisons

Following the LCL filter design principles in [7], a three-port dc hub is designed. The topology of VSCs used in this case is half-bridge single-phase two-level VSC. The parameters of the hub components are listed in Table I and other specifications are listed in Table II. The parameters of PI controllers used are listed in Table III.

In [7], it is stated that the switching frequency can be as low as three times the fundamental frequency. However, under this situation the current harmonics bring significant oscillations into the *dq* components. This makes it challenging to properly respond to the changes in the dc hub as the filters in the control system need a very large time constant to smooth the *dq* component of the current.

TABLE I
POWER CIRCUIT COMPONENTS OF THE THREE-PORT DC HUB

L_1 (H)	L_2 (H)	L_3 (H)	C_{eq} (μF)	R_1 (Ω)	R_2 (Ω)	R_3 (Ω)
0.0103	0.0154	0.0178	2.0465	0.5	0.5	0.5

TABLE II
SPECIFICATIONS OF THE THREE-PORT DC HUB

Port 1	Rated maximum power	150 MW
	DC link voltage	±150 kV
Port 2	Rated maximum power	-100 MW
	DC link voltage	±100 kV
Port 3	Rated maximum power	-50 MW
	DC link voltage	±50 kV
Fundamental frequency		1.25 kHz
Switching frequency		11.25 kHz

TABLE III
PARAMETERS OF PI CONTROLLERS OF THE THREE-PORT DC HUB

PI	I_{1d}	I_{1q}	I_{2d}	I_{2q}	I_{3d}	I_{3q}	P_2	P_3
K_p	0.05	0.05	0.05	0.05	0.05	0.05	10^{-4}	10^{-4}
T_i ($1/K_i$)	0.06	0.4	0.4	2	0.4	0.5	200	200
Upper Limit	1	1	1	1	1	1	0	0
Lower Limit	-1	0.01	-1	0.01	-1	0.01	-3	-3

A. Comparison of Simulation Results

The three-port dc hub with closed loop control is simulated in PSCAD/EMTDC (detailed EMT simulation) and its results are used to benchmark the accuracy and computational advantage of the developed average-value model (implemented in MATLAB). Both models are run for a simulation time period of 10 s. The time-step used in the EMT model is 0.1 μs, which is necessary to have proper representation of the switching converters. For the simulation of developed average-value model, a time-step of 1000 μs is selected to ensure the numerical stability and simulation accuracy. In the EMT model, the integration method is trapezoidal rule. For the integration of the averaged model, the state equations are solved by the trapezoidal rule and the control system is solved using Euler's method.

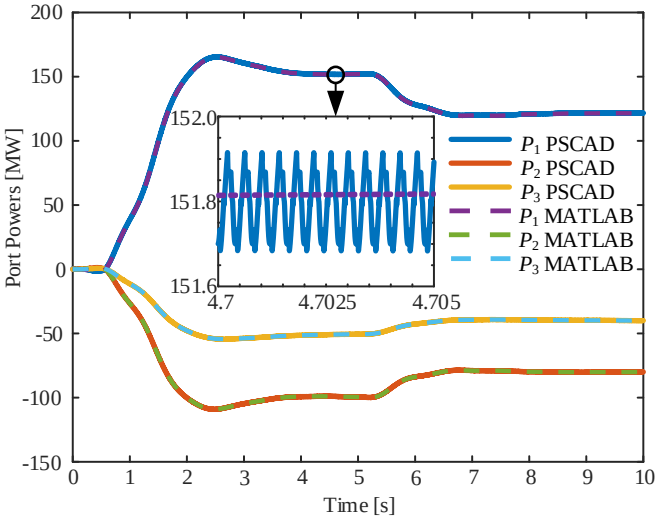

Fig. 5. Simulation results of port powers.

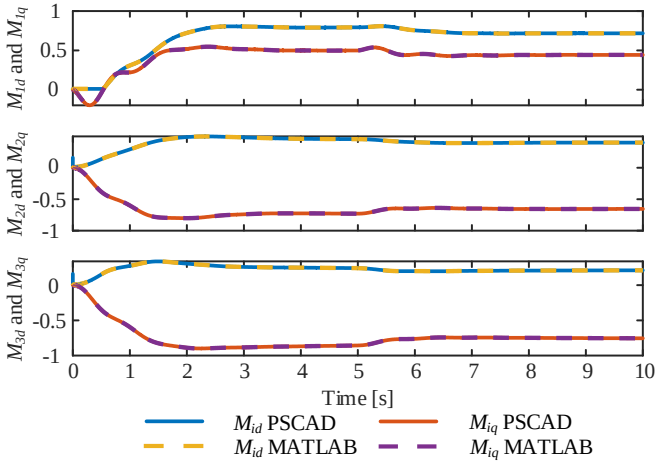

Fig. 6. Simulation results of *dq* components of modulation indices.

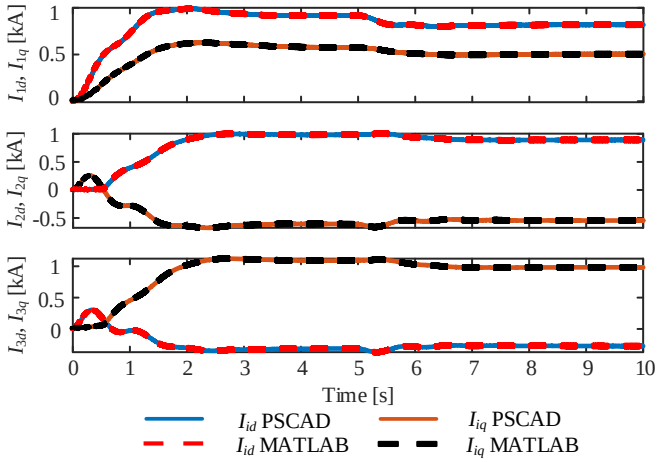

Fig. 7. Simulation results of filtered *dq* components of port currents.

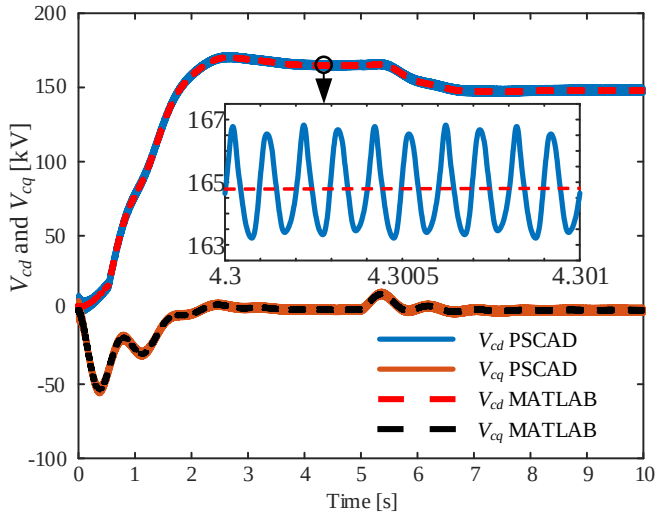

Fig. 8. Simulation results of *dq* components of V_C.

Figs. 5-8 show comparisons of the simulation results, including port powers, *dq* components of modulation indices, port currents, and capacitor voltage. Simulation results from both the EMT and the average-value model match closely, which validates the accuracy of the proposed average model.

As indicated in Section II.B, there are only two references for the 3-port system. In the simulations, power references are initially set to -100 MW and -50 MW for ports 2 and 3, respectively. To verify the dynamics of the averaged model under the proposed control method shown in Fig. 2, step changes in power references are applied at t = 5 s to ports 2 and 3, which drop to -80 MW and -40 MW, respectively. As shown in Fig. 5 to Fig. 8, the system quickly responds to these step changes and the dc signals of corresponding *dq* components settle to the desired values using both models. The insets in Figs. 5 and 8 show closer views of the EMT and average-value models and depict the low-amplitude, high-frequency contents that are ignored in the average-value model. Therefore, the proposed control method for multiport dc hub is effective, and the averaged model accurately represents the system operation with a much larger time-step.

B. Simulation Efficiency

The simulations using these two models are performed on the same computer. Computational efficiency is summarized in Table IV. Without noticeable loss of accuracy, the simulation speed of the proposed average model is clearly faster than the EMT model due to the significantly larger time-steps that may be used in this model. The simulation time-steps shown in Table IV are the largest values for each simulator to produce accurate results. As seen the developed average-value model is in more than 600 times faster than the EMT model, yet produces results of virtually identical quality. It must be noted that the two models are implemented in markedly different computing environments. The average-value model is implemented in MATLAB, whereas the EMT model is in PSCAD/EMTDC. MATLAB is a far slower platform than the FORTRAN-based EMTDC solver; despite this disadvantage, the average-value model outperforms that EMT model significantly, even though it is not a complied model. If the two models are implemented in the same environment, the computational advantage of the average value model will be even more pronounced.

TABLE IV
SIMULATION EFFICIENCY COMPARISON

Model	Simulation time-step	CPU time of computations
PSCAD/EMTDC	0.1 μs	about 450 s
Averaged Model	1000 μs	0.67 s

C. AC Waveform Recovery

Due to the large time-step used in the simulation of the proposed model, recovery of the ac waveforms for display purposes needs special attention. Since the fundamental frequency is high, there will not be sufficient data points to show the ac waveforms using the granular data points in the respective *dq* quantities. To obtain the ac waveforms, an ac waveform recovery method is used. As a rule of thumb, the largest time-step that can be used in simulation is

$$t_{largest} \le \frac{1}{10} \times \frac{1}{f_{highest}} \tag{19}$$

where $f_{highest}$ is the largest harmonic component of interest. For instance, a 1.25 kHz ac system may be simulated with a time-step no larger than 80 μs. With more points within one cycle, ac waveforms can be recovered more accurately. To recover

an ac waveform, it is possible to insert more data points in its *dq* components before conversion to the *abc* frame. The computation of the inserted data points can be approximately decided based on the slope and the values between two original points. For example, in a dc waveform, suppose that there are two points (d_1 and d_2), and the time-step is Δt_1. If the required time-step for displaying the ac waveforms is Δt_2, then the number of data points to be inserted between d_1 and d_2 is,

$$n = \frac{\Delta t_1}{\Delta t_2} - 1 \tag{20}$$

The inserted data points can be computed as

$$d'_i = i\frac{d_2 - d_1}{\Delta t_1}\Delta t_2, i = 1, 2, ..., n \tag{21}$$

Using this method, the capacitor voltage and port currents are recovered from *dq* components and compared to the simulation results obtained from the EMT model, as shown in Fig. 9 and 10. It is observed from Fig. 9 that the original V_C envelope waveform computed by the proposed average model does not display a sinusoidal waveform, while the recovered capacitor voltage waveform in MATLAB matches well to the result from the detailed EMT model. In Fig. 10, with the same recovery method, the recovered current waveforms show excellent fit into the detailed simulation results. The port currents do not completely match with the PSCAD/EMTDC solution is because this method only provides allowance to display the fundamental ac waveform since the proposed average model only simulates the fundamental component. Nevertheless, by adding more harmonics this method will provide adequately accurate representations of ac waveforms.

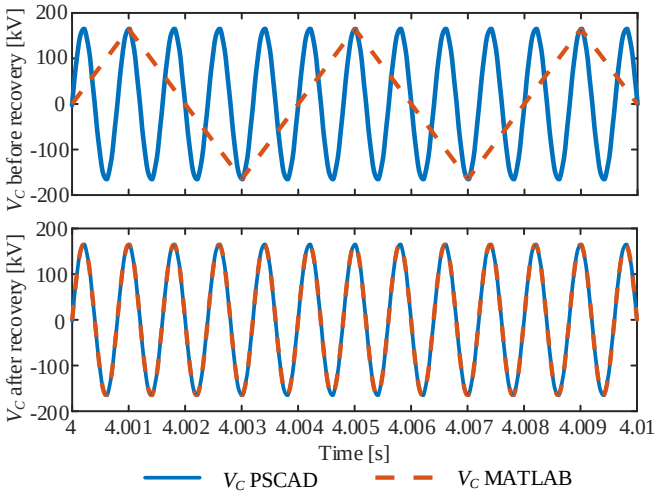

Fig. 9. Comparison of V_C waveforms obtained from EMT simulation and averaged model without and with recovery method.

V. Conclusions

Based upon the principle of dynamic phasors, this paper proposed the averaged model of a multiport dc hub to reduce the computational cost of its simulation. A three-port dc hub was designed and modeled using the average values of *dq* components. Compared with the EMT simulation results, the averaged model, with a large time-step, showed high accuracy to simulate the *dq* components of operating signals in dc hub under both steady-state and dynamic operations. This validated the benefits of the averaged model (high accuracy and computational efficiency) to study the operation and dynamic behaviors of dc hub. Additionally, an ac waveform recovery method was introduced for displaying high-resolution ac waveform, since averaged model is generally simulated with large time-steps.

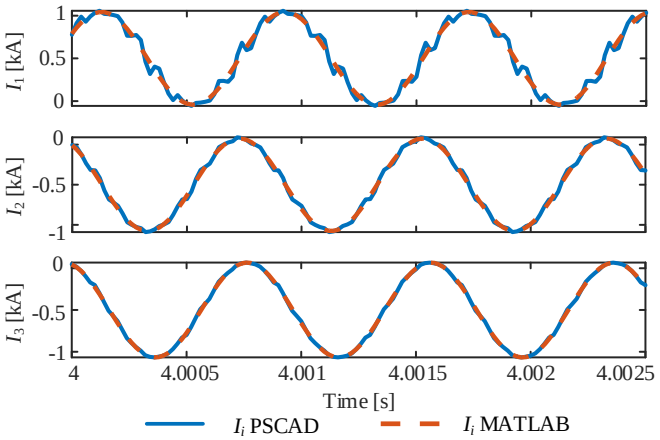

Fig. 10. Comparison of port currents obtained from EMT simulation and averaged model without and with recovery method.

VI. References

[1] R. W. A. A. De Doncker, D. M. Divan and M. H. Kheraluwala, "A three-phase soft-switched high-power-density DC/DC converter for high-power applications," *IEEE Trans. on Ind. Applications*, vol. 27, no. 1, pp. 63-73, Jan/Feb 1991.

[2] Y. Xie, J. Sun and J. S. Freudenberg, "Power Flow Characterization of a Bidirectional Galvanically Isolated High-Power DC/DC Converter Over a Wide Operating Range," *IEEE Trans. on Power Electronics*, vol. 25, no. 1, pp. 54-66, Jan. 2010.

[3] S. Kenzelmann, A. Rufer, D. Dujic, F. Canales and Y. R. de Novaes, "A versatile DC/DC converter based on Modular Multilevel Converter for energy collection and distribution," in *Proc. IET Conference on Renewable Power Generation*, Edinburgh, 2011.

[4] O. Abutbul, A. Gherlitz, Y. Berkovich and A. Ioinovici, "Step-up switching-mode converter with high voltage gain using a switched-capacitor circuit," *IEEE Trans. on Circuits and Systems I: Fundamental Theory and Applications*, vol. 50, no. 8, pp. 1098-1102, Aug. 2003.

[5] W. Chen, A. Q. Huang, C. Li, G. Wang and W. Gu, "Analysis and Comparison of Medium Voltage High Power DC/DC Converters for Offshore Wind Energy Systems," *IEEE Trans. on Power Elect.*, vol. 28, no. 4, pp. 2014-2023, April 2013

[6] G. J. Kish, M. Ranjram and P. W. Lehn, "A Modular Multilevel DC/DC Converter With Fault Blocking Capability for HVDC Interconnects," *IEEE Trans. on Power Elect.*, vol. 30, no. 1, pp. 148-162, Jan. 2015.

[7] D. Jovcic and W. Lin, "Multiport High-Power LCL DC Hub for Use in DC Transmission Grids," *IEEE Trans. on Power Delivery*, vol. 29, no. 2, pp. 760-768, April 2014.

[8] D. Jovcic and L. Zhang, "LCL DC/DC Converter for DC Grids," *IEEE Trans. on Power Delivery*, vol. 28, no. 4, pp. 2071-2079, Oct. 2013.

[9] S. M. Fazeli, D. Jovcic and M. Hajian, "Laboratory Demonstration of Closed-Loop 30 kW, 200 V/900 V IGBT-Based LCL DC/DC Converter," *IEEE Trans. on Power Delivery*, vol. 33, no. 3, pp. 1247-1256, June 2018.

[10] W. Lin and D. Jovcic, "Average Modelling of Medium Frequency DC–DC Converters in Dynamic Studies," *IEEE Trans. on Power Delivery*, vol. 30, no. 1, pp. 281-289, Feb. 2015.

[11] S. R. Sanders, J. M. Noworolski, X. Z. Liu and G. C. Verghese, "Generalized averaging method for power conversion circuits," *IEEE Trans. on Power Elect.*, vol. 6, no. 2, pp. 251-259, April 1991.